JOURNAL OF SOLID STATE CHEMISTRY 73, 488–501 (1988)

Physicochemical Properties of Dy^{3+} in Single $KY(MoO_4)_2$ Crystal (Electron Absorption, Emission, IR, Raman, and Magnetic Data)

J. HANUZA, L. MACALIK, W. RYBA-ROMANOWSKI, E. MUGEŃSKI, AND R. CYWIŃSKI

Institute for Low Temperature and Structure Research, Polish Academy of Sciences, 50-950 Wrocław, Poland

AND K. WITKE, W. PILTZ, AND P. REICH

Institute of Physical Chemistry, Academy of Sciences of the German Democratic Republic, Berlin, German Democratic Republic

Received November 18, 1986; in revised form September 14, 1987

Electron absorption, luminescence, vibrational, and magnetic properties of $KDy_xY_{1-x}(MoO_4)_2$ crystals are examined over the entire concentration region $x = 0$ to $x = 1$ and a temperature range 13–293 K. The crystal field scheme of the ^6H, ^6F, ^4F, ^4I manifolds and their Stark components are established. The τ_λ Judd–Ofelt parameters are determined by the numerical method and related to the concentration effect. The temperature dependence of the lifetime of luminescence is discussed and a quenching mechanism is proposed. © 1988 Academic Press, Inc.

Introduction

The Dy^{3+}-doped inorganic crystals have been considerably less thoroughly investigated compared to other rare-earth elements in crystalline hosts. Dysprosium-containing materials have been found to be less attractive for application in laser devices working in the visible or near infrared region. Recently, however, interest in laser material engineering has been directed toward the crystals which would work in the 3000 cm^{-1} wavelength region and here the Dy^{3+}-doped crystals offer a unique property that makes it possible to obtain the laser action using the $^6H_{13/2}$–$^6H_{15/2}$ transition (*1*). In order to achieve the best ion–host combination the spectroscopic behavior of the Dy^{3+}-doped materials should be known in detail and such information is very scarce.

In the present paper we discuss the spectroscopic and magnetic properties of the $KDy_xY_{1-x}(MoO_4)_2$ crystals. The double molybdates doped with neodymium have proved their usefulness as efficient laser materials (*2*). We believe that this paper will contribute to the knowledge of Dy^{3+}-containing materials and will help in a search for new laser crystals working in the near infrared region.

Experimental

The single $KY(MoO_4)_2$, $KDy(MoO_4)_2$, and $KDy_xY_{1-x}(MoO_4)_2$ crystals were grown

0022-4596/88 $3.00

from the melt using the method described by Klevtsova *et al.* (*3*). The room-temperature absorption spectra were measured on Perkin–Elmer 180 and Cary 14 spectrophotometers. The fluorescence spectra at 300 and 77 K were measured on a spectrometer designed in our laboratory, using a Carl Zeiss GDH 1000 grating monochromator equipped with a phase-sensitive detection system. Fluorescence was excited using a 478-nm line and a 458-nm line of an argon ion ILA 120 laser and detected by cooling photomultipliers with S-1 and S-11 response, depending on the spectral region.

For decay curve analysis a broad band excitation source consisting of a xenon flashlamp and appropriate filters was used. The excitation wavelengths were chosen to match the strong absorption bands situated between 20,000 and 30,000 cm^{-1}, corresponding to the transitions from the $^6H_{15/2}$ level to the $^4F_{7/2}$, $^4M_{19/2}$, $^6P_{5/2}$, $^4I_{11/2}$, and $^6P_{7/2}$ levels of Dy^{3+} ions. The resulting decays of luminescence from the $^4F_{9/2}$ level were analyzed by means of a ZWG boxcar integrator Model BCI 280. In all measurements the $^4F_{9/2}$–$^6H_{13/2}$ transition was monitored.

The IR and Raman spectra were recorded in a Perkin–Elmer 180 spectrophotometer and JEOL S1 spectrometer, respectively.

The magnetic susceptibility measurements were made by the Faraday method over the range 4.2–300 K. The forces acting upon the crystal were measured on a high-vacuum Cahn RH electronic balance. The $KDy(MoO_4)_2$ crystal was placed in a modified sample holder used for measurements of powders and suspended under helium atmosphere at the pressure of a 100-mm oil column. Magnetic susceptibility measurements of a crystal were taken in three directions by placing it in the magnetic field in positions parallel to the three axes, i.e., *a*, *b*, and *c* of the crystal. All measurements were performed at the magnetic field intensity, in the point where the sample was located, equal to 6250 G. Diamagnetic corrections were not applied to the data because these corrections were less than 1% of a crystal susceptibility. The estimated absolute accuracy of the susceptibility measurements is within 2%.

Results and Discussion

Infrared and Raman Spectra

According to the results of the structural analysis (*3*) the room temperature phases of $KDy(MoO_4)_2$ and $KY(MoO_4)_2$ are isostructural belonging to the orthorhombic space group $D_{2h}^{14} = Pbcn$ with $Z = 4$. Both of these crystals present a multilayer structure of scheelite type which consists of chains containing eight-coordinated DyO_8 and YO_8 polyhedra elongated along the *c*-axis and connected through edges. These chains are connected through the MoO_4 tetrahedra, which additionally join DyO_8 or YO_8 polyhedra in particular chains. In such a structure the Y^{3+} ions may be substituted by Dy^{3+} ions totally or partially without any modification of the crystal structure and Dy^{3+} site symmetry. This observation is fully confirmed by the IR, Raman, near infrared (NIR), UV–VIS, and emission measurements performed on the stoichiometric $KDy(MoO_4)_2$, $KY(MoO_4)_2$, and diluted $KDy_xY_{1-x}(MoO_4)_2$ crystals. The IR and Raman spectra of these materials are presented in Figs. 1 and 2 and described in Table I.

The detailed vibrational analysis of the single $KY(MoO_4)_2$ and $KDy(MoO_4)_2$ crystals using polarized light and oriented samples was performed by us previously (*4*). In this paper we report on the concentration dependence and temperature behavior of the optical modes. The typical composition dependence of the low-frequency IR and Raman spectra are shown in Fig. 2 for arbitrary intensity normalizations. The remarkable feature in these spectra con-

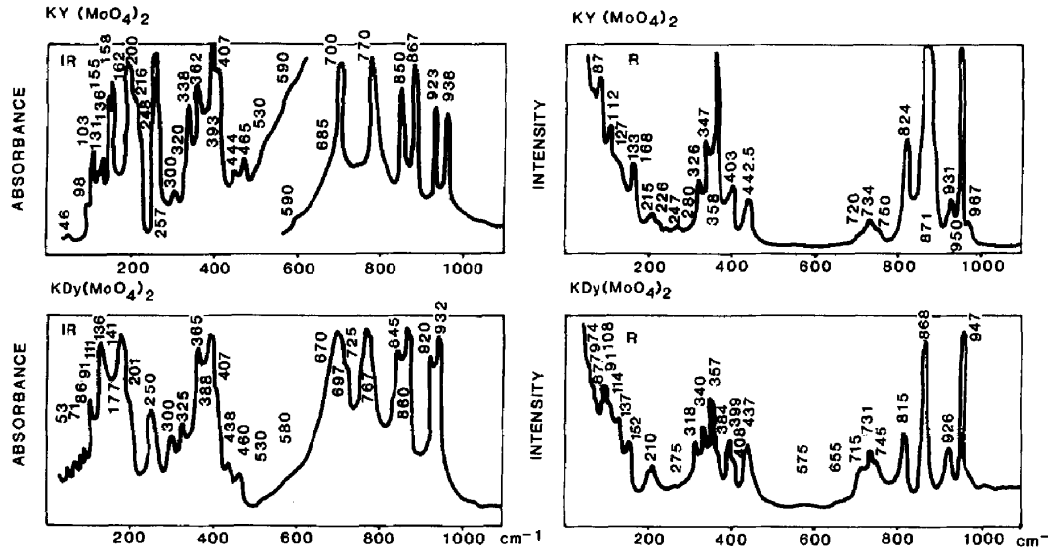

FIG. 1. IR and Raman spectra of $KY(MoO_4)_2$ and $KDy(MoO_4)_2$.

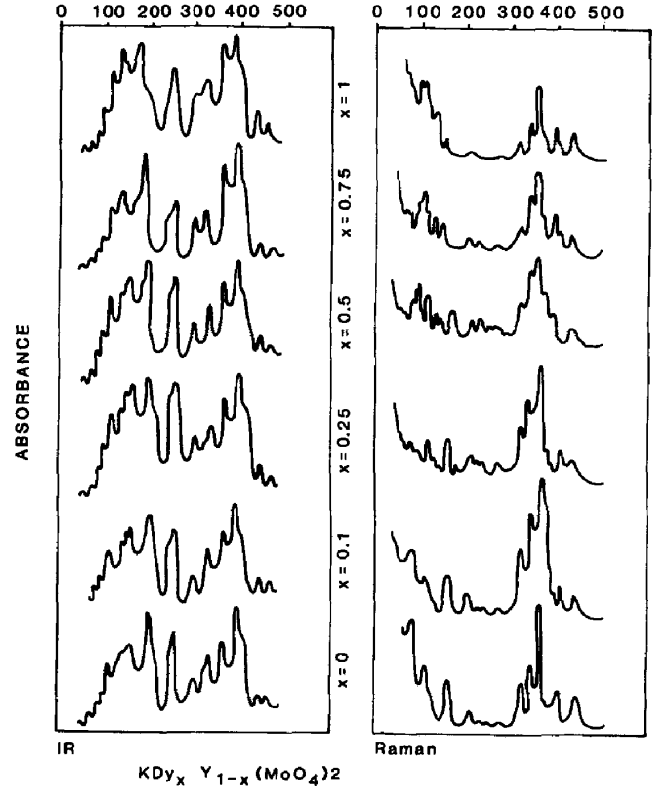

FIG. 2. Low-frequency IR and Raman spectra of $KDy_xY_{1-x}(MoO_4)_2$ for different compositions x. The spectra are vertically shifted by different amounts.

TABLE I

THE WAVENUMBERS FOR $KY(MoO_4)_2$ AND $KDy(MoO_4)_2$ OBTAINED AT 12 K (IR SPECTRA) AND 70 K (RAMAN SPECTRA)

$KDy(MoO_4)_2$				$KY(MoO_4)_2$			
IR [cm^{-1}]		Raman [cm^{-1}]		IR [cm^{-1}]		Raman [cm^{-1}]	
12 K	293 K	70 K	293 K	12 K	293 K	70 K	293 K
		36				38	
41,67	53	40		47	46	39	
		59				56	
			74				
72	71	75	79				
88	86	81	87				
93	91	89	94				
		98		100	98	88	87.5
		101	108	105	104	105	
113	111	106	114	111	109	109	
122		118		126	124	113	112
136	136	130	126	133	131	130	127
143	141	135	137	140	138	134	133
		149				148	
163	161	154	152	158	155		
179	177			160	158		
203	201	211	210	164	162	167,178	168
		217		202	202		
227	223	226	225	218	216	211,221	215
254	250	238	238	251	248	226	226
285	282	277	275	261,272	257	249	247
303	300			289,302	300	282	280
312				311,322	320	328	326
328	325	320	318	336,349	338	345	343
345		342	340	367	362	360,386	358
369	365	354,363	357	396,398	393		
391	388	385	384	410,414	407	504,410	403
398		399	399	447	444	444	442.5
410	407	411	408	469	465		
441	438	439	437	533		530	
448				593		557	
463	460					610	
535		530				675	
584	580	576		704	700	723	720
683		655				737	734
699	697	711	715	774	770	753	750
728	725	738	731				
770	767	747	745				
		812	815				
850	845	853		854	850	827	824
864	860	870	868	871	867	874	871
924	920	928	926	928	923	934	931
935	932	949	947	943	938	953	950
						971	967

cerns the stability of the spectral profile with varying composition. The band positions of stoichiometric and diluted samples are very close to each other in the full-frequency range except for the low-frequency region near 130–200 cm^{-1}. The bands at 190 and 160 cm^{-1} observed for $KY(MoO_4)_2$ are gradually replaced by doublet contours when the Dy^{3+} concentration is increased. The fully concentrated $KDy(MoO_4)_2$ sample reveals the single bands at 160 and 130 cm^{-1} in this place. These bands are connected with the translational lattice $T'(Ln^{3+})$ modes since behavior like this is characteristic for the *RE*–oxygen systems (*4*).

The temperature dependence of the IR and Raman frequencies for the systems under investigation is illustrated in Table I.

The IR and Raman spectra obtained here for $KY(MoO_4)_2$ and $KDy(MoO_4)_2$ crystals at liquid helium temperature are in many points similar to those measured at room temperature when the band contours and spectral pattern are compared. The differences result from the temperature band shifts (5–10 cm^{-1}) and splittings of the unresolved bands. It must be noted, however, that low-temperature spectra have revealed the existence of a few new bands in the region 480–700 cm^{-1} both for yttrium and dysprosium molybdates. In previously measured room-temperature spectra (*4*) these lines were observed on the slope of intense neighbor bands as shoulders or as isolated very weak bands; therefore, they seem to be two-phonon (internal–external combination modes) transitions. Low-temperature study indicates, however, that because of their intensities these bands should be considered as internal modes. In our previous papers (*4*) dealing with spectroscopic studies of single $KLn(MoO_4)_2$ crystals we have found that the discrepancies between the spectroscopic observables and the selection rules for a structural model suggested by X-ray analysis result from additional interactions in the unit cell. These interactions between the molybdate ions lead to the formation of the dimeric Mo_2O_8 systems containing oxygen bridge bonds:

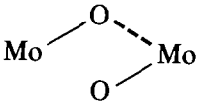

LHe-temperature studies indicate that these Mo_2O_8 dimers are coupled by means of next oxygen bridges forming the polymeric ribbon. The repeated fragment of this ribbon is formed by two MoO_6 octahedra, each of them built from four short (1.72–1.83 Å) and two long (2.73 Å) molybdenum–oxygen distances. That problem is the subject of a separate consideration (*5*).

Electronic Absorption Spectra

The room-temperature absorption spectra of $KDy_xY_{1-x}(MoO_4)_2$ in the region 3000–30,000 cm^{-1} are presented in Fig. 3.

The number of multiplet terms for the f^9 configuration equals 73; the number of levels with various J is 198; the ground level of Dy^{3+} is $^6H_{15/2}$. Interpretations of the Dy^{3+} crystal spectra have been reported (*6, 7*). Carnall *et al.* (*8*) have analyzed theoretically the dysprosium(III) aquo-ion absorption spectra and have assigned spectral bands up to 40,000 cm^{-1}. The f–f transitions of Dy^{3+} with energy higher than 36,000 cm^{-1} are superimposed by more intense absorption due to the MoO_4^{2-} charge transfer. The oscillator strengths of bands in the absorption spectra of Dy^{3+} in solutions have been given (*8–10*). In the visible spectral region hypersensitive transitions are not observed. A hypersensitive band was found (*11*) in the NIR region at 7700 cm^{-1} and assigned to the $^6H_{15/2} \rightarrow {}^6F_{11/2}$ transition.

All literature date cited here were the basis for analysis and assignment of results obtained by us. The room temperature absorption spectrum of Dy^{3+} in $KY(MoO_4)_2$

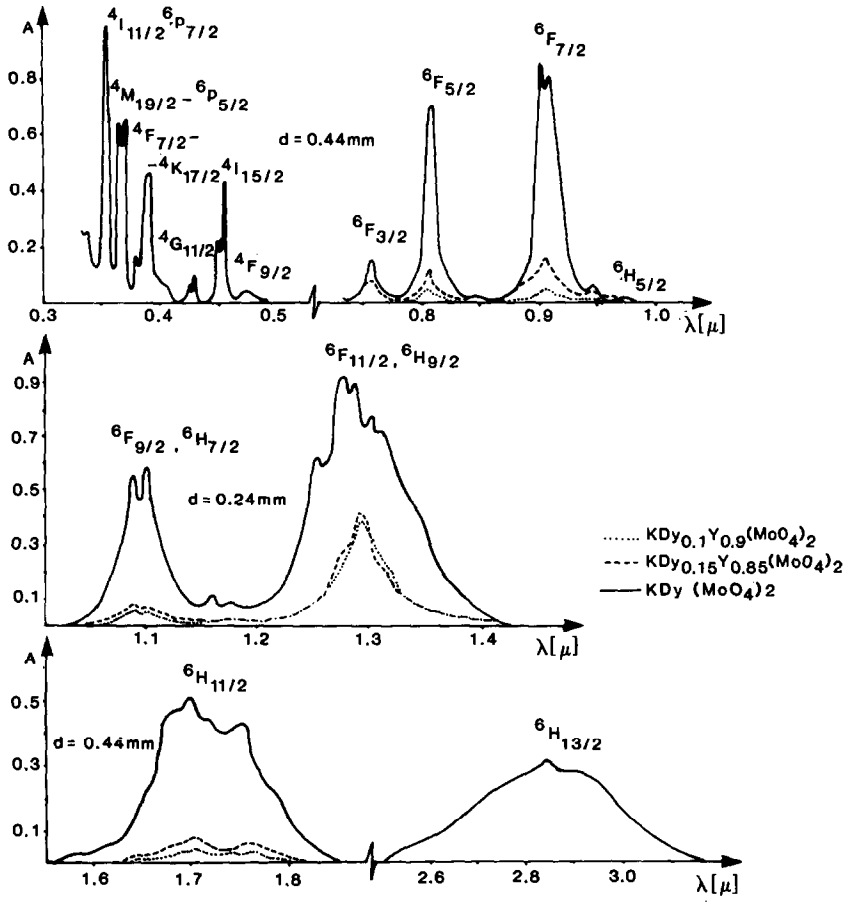

FIG. 3. The absorption spectra of $KDy_xY_{1-x}(MoO_4)_2$ crystals (x = 1, 0.15, 0.1) in the range 3000–30,000 cm^{-1}.

consists of groups of lines centered at 29,000–24,200, 23,700–20,400, 12,900–11,500, 11,500–10,300, 9700–8400, 8400–6800, 6400–5200, and 4000–3100 cm^{-1} (Fig. 3) corresponding to the transitions from the $^6H_{15/2}$ ground level to the excited states of the $4f^9$ configuration. The IR and NIR bands situated within the region 3100–12,900 cm^{-1} correspond to the low-energy transitions to the excited levels of the ground ^6H manifold and to the low-lying levels of the ^6F sextet. The next group of bands in the VIS and UV correspond to the transitions to the closely spaced quartet ^4F, ^4I, ^4G, ^4K, ^4H, and sextet ^6P states. Detailed identification of transitions observed in the absorption spectrum and corresponding oscillator strength values obtained by numerical integration of absorption band contours are given in Table II. The oscillator strength values were evaluated theoretically by a fitting procedure following the Judd–Ofelt theory using the expression introduced by Peacock (*12*). Resulting τ_λ parameters for Dy^{3+} in $KDy_xY_{1-x}(MoO_4)_2$ are listed in Table III. The oscillator strengths were determined using the equations,

$$P = \sum_{\lambda} \tau_\lambda \sigma \, |\langle 4f^N \| U^{(\lambda)} \| 4f^{N\prime} \rangle|^2/(2J + 1), \qquad \lambda = 2, 4, 6,$$

TABLE II

THE ENERGY POSITIONS AND OSCILLATOR STRENGTH VALUES OF f–f TRANSITIONS FOR $KDy_{0.25}Y_{0.75}(MoO_4)_2$ CRYSTALS

Energy level	Spectral range λ [cm^{-1}]	Wave number σ [cm^{-1}]	$P_{exp} \times 10^8$	$P_{calc} \times 10^8$
$^6H_{11/2}$	6,452– 4,902	5,889	249.97	203.42
$^6F_{11/2}$	8,439– 7,018	8,000	1305.59	1310.73
$^6H_{9/2}$				
$^6F_{9/2}$	9,756– 8,439	9,191	359.82	415.43
$^6H_{7/2}$				
$^6H_{5/2}$	10,417– 9,756	10,152	10.29	0.86
$^6F_{7/2}$	11,561–10,417	11,062	313.67	313.58
$^6F_{5/2}$	12,903–11,561	12,407	166.28	140.33
$^6F_{3/2}$	13,605–12,903	13,245	29.44	26.44
$^4F_{9/2}$	21,505–19,704	20,986	34.22	23.83
$^4I_{15/2}$	22,727–21,505	21,978	116.89	68.65
$^4G_{11/2}$	23,952–22,727	23,310	39.56	13.71
$^4F_{7/2}$,$^4L_{13/2}$	26,702–23,923	25,853	341.65	330.64
$^4M_{21/2}$,$^4K_{17/2}$				
$^4M_{19/2}$, (^4P,$^4D)_{3/2}$,$^6P_{5/2}$	27,624–26,702	27,274	203.58	210.48
$^4I_{11/2}$,$^6P_{7/2}$	29,028–27,624	28,409	574.90	555.98

where $U^{(\lambda)}$ are double-reduced matrix elements for tensor operators, τ_λ is the phenomenological parameter, and σ is the center of gravity for the absorption band in cm^{-1}.

The concentration behavior of τ_2, τ_4, and τ_6 parameters evaluated here is given in Fig. 4. The τ_4 and τ_6 values seem not to be sensitive to concentration changes. On the other hand, the τ_2 parameter exhibits strong concentration dependence since in the low-concentration range (0.0–0.25) its relationship shows a strong decrease and above a 0.25 Dy^{3+} content it becomes nonlinear.

Luminescence Properties

The energy level diagram of the Dy^{3+} ion in $KY(MoO_4)_2$ is given in Fig. 5. Under 478- and 458-nm laser excitation at 77 and 300 K the strong fluorescence consisting of groups of lines centered is observed in the visible and near infrared at 21,000, 17,500, 15,200, 13,300, and 12,000 cm^{-1}. These lines represent transitions from $^4F_{9/2}$ terminating on $^6H_{15/2}$, $^6H_{13/2}$, $^6H_{11/2}$, ($^6F_{11/2}$, $^6H_{9/2}$), and ($^6H_{7/2}$, $^6F_{9/2}$), respectively.

Although Dy^{3+} in $KDy_xY_{1-x}(MoO_4)_2$ presents a great number of absorbing levels in the 20–30 $\times$ 10^3 cm^{-1} region, only the $^4F_{9/2}$ level shows notable fluorescence in the VIS and NIR. This feature is due to small energy gaps between adjacent successive levels. These gaps do not exceed 10^3 cm^{-1}. On the other hand the crystal host exhibits very rich phonon spectrum with the cutoff frequency corresponding to molybdenum–

TABLE III

THE JUDD–OFELT INTENSITY PARAMETERS OF Dy^{3+} IN $KDy_xY_{1-x}(MoO_4)_2$ CRYSTALS

	$x = 1.0$	$x = 0.75$	$x = 0.25$	$x = 0.15$	$x = 0.1$	$x = 0.02$
$\tau_2 \times 10^9$	15.979 ± 0.60146	19.587 ± 0.66852	21.281 ± 0.78915	34.923 ± 1.4520	52.411 ± 1.6075	66.683 ± 1.8516
$\tau_4 \times 10^9$	6.5018 ± 0.26153	5.8791 ± 0.29279	5.8098 ± 0.34797	8.3828 ± 0.63453	8.3405 ± 0.70554	5.0582 ± 0.81923
$\tau_6 \times 10^9$	5.2661 ± 0.29129	5.3289 ± 0.32173	5.1738 ± 0.38399	4.0457 ± 0.69720	2.6837 ± 0.77498	7.7457 ± 0.90356
$S \times 10^7$	0.1548	0.1745	0.20641	0.3777	0.4201	0.4844

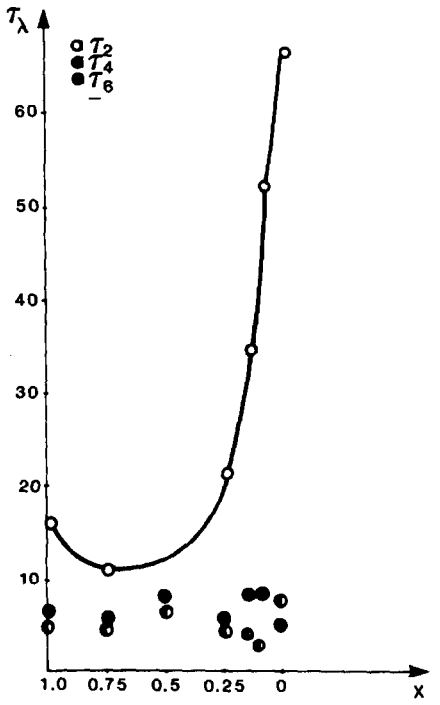

FIG. 4. The concentration dependence of Judd–Ofelt $\tau_{2,4,6}$ parameters for $KDy_xY_{1-x}(MoO_4)_2$.

oxygen stretching vibrations at about 900 cm^{-1} (Fig. 1, Table I). Therefore, all higher lying levels are depopulated very quickly by an efficient nonradiative relaxation leading to the population of the $^4F_{9/2}$ level separated from the next lower lying level by about 6000 cm^{-1}. The $^4F_{9/2}$ level is depopulated by radiative transitions and/or concentration quenching mechanisms because of a large energy gap. The room and liquid nitrogen temperature fluorescence spectra associated with the radiative transitions from the $^4F_{9/2}$ level of Dy^{3+} are shown in Figs. 6 and 7.

It is interesting to note that the intensities of observed transitions are roughly comparable at both temperatures. This implies that the corresponding fluorescence branching ratios are of similar magnitude. The lowering of the crystal temperature to 77 K enables the observation of the transitions between individual crystal field components of levels involved, which, in relation to the absorption spectra observed, permits the determination the Stark splittings. The energy levels of Dy^{3+} in crystals studied are listed in Table IV.

The concentration quenching of Dy^{3+} luminescence was found to be very efficient in $KDy_xY_{1-x}(MoO_4)_2$ crystals (see Fig. 8). In the case of diluted crystals, i.e., for $x < 0.1$, single exponential decay was observed, and the measured decay times as well as the integrated luminescence intensity diminished with increasing concentration of Dy^{3+} ions. For higher Dy^{3+} concentrations the luminescence decay curves cannot be described by single exponential dependence. This observation indicates the importance of ion–ion interactions which should be responsible for the quenching of luminescence from the $^4F_{9/2}$ level. The multiphonon relaxation seems to be negligible remembering that the next lower lying level is situated at about 13,000 cm^{-1}. More than seven phonons of maximum energy in this host would be needed to cover such an

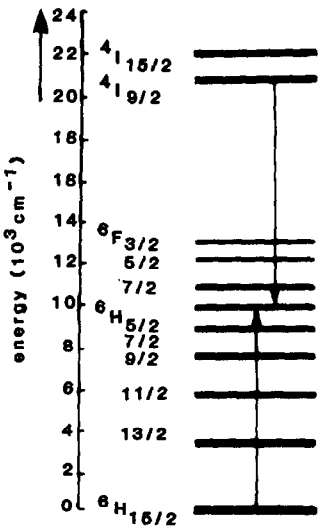

FIG. 5. Energy level diagram of Dy^{3+} ion. Crystal-field components are not shown. Energies in cm^{-1}. Arrows indicate the cross-relaxation process. Only a part of the higher energy levels is shown.

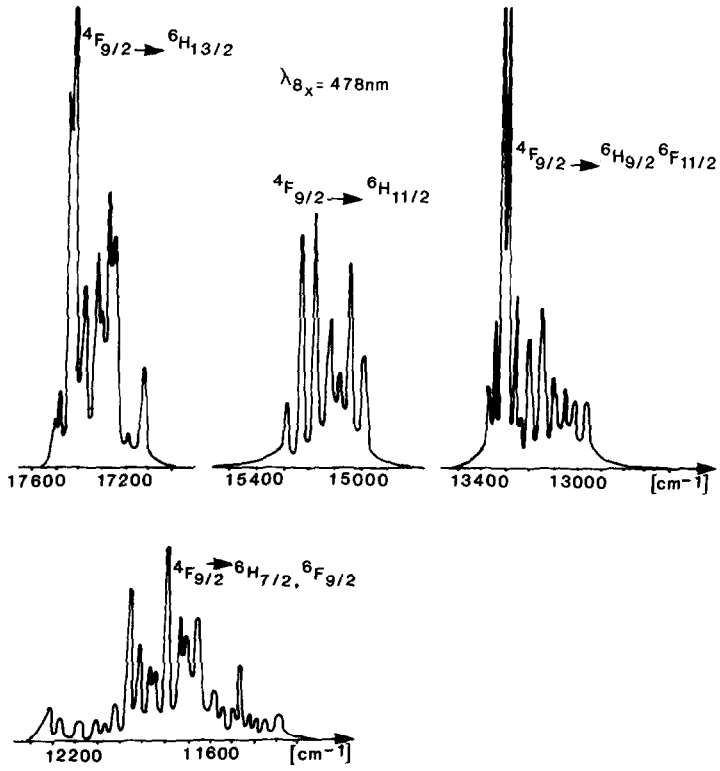

FIG. 6. Fluorescence spectra of the $KDy_{0.1}Y_{0.9}(MoO_4)_2$ crystal at 77 K.

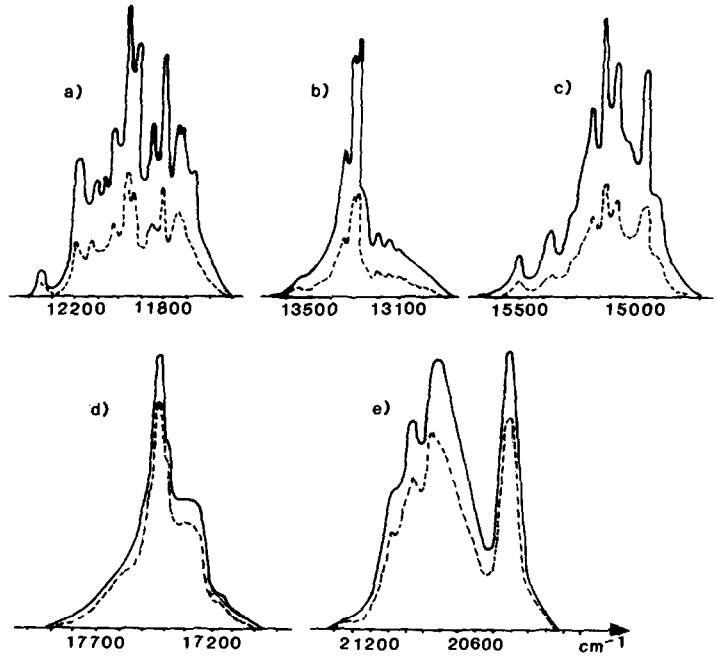

FIG. 7. Fluorescence spectra of the $KDy_xY_{1-x}(MoO_4)_2$ crystals at room temperature ($x = 0.1$ (—), $x = 0.15$ (– – –)): (a) $^4F_{9/2} \rightarrow {}^6H_{7/2}$, $^6F_{9/2}$, $\lambda_{ex} = 458$ nm; (b) $^4F_{9/2} \rightarrow {}^6H_{9/2}$, $^6F_{11/12}$, $\lambda_{ex} = 458$ nm; (c) $^4F_{9/2} \rightarrow {}^6H_{11/2}$, $\lambda_{ex} = 458$ nm; (d) $^4F_{9/2} \rightarrow {}^6H_{13/2}$, $\lambda_{ex} = 458$ nm; (e) $^4F_{9/2} \rightarrow {}^6H_{15/2}$, $\lambda_{ex} = 458$ nm.

TABLE IV
ENERGY LEVELS OF Dy^{3+} IN $KDy_xY_{1-x}(MoO_4)_2$

Level	Stark components	Component theor.	Number exper.	ΔE
$^6H_{13/2}$	3,520; 3,565; 3,630; 3,660; 3,710; 3,760; 3,810	7	7	290
$^6H_{11/2}$	5,814; 5,882; 5,952; 6,000; 6,061	6	5	247
$^6H_{9/2}$	7,587; 7,648; 7,669; 7,692; 7,752	5	5	165
$^6F_{11/2}$	7,828; 7,927; 7,978	6	3	150
$^6H_{7/2}$	8,929; 8,998; 9,050; 9,099	4	4	170
$^6F_{9/2}$	9,170; 9,217; 9,260; 9,302; 9,390	5	5	220
$^6H_{5/2}$	10,165; 10,256; 10,336	3	3	171
$^6F_{7/2}$	10,935; 11,004; 11,042; 11,086	4	4	151
$^6F_{5/2}$	12,415; 12,469; 12,500	3	3	85
$^6F_{3/2}$	13,201; 13,233	2	2	32
$^4F_{9/2}$	20,975; 21,008; 21,053; 21,166	5	4	191
$^4I_{15/2}$	21,968; 22,112; 22,173; 22,272	8	4	304

energy gap. Therefore, we can assume safely that the radiative lifetime of the $^4F_{9/2}$ level is close to 240 μsec, the value measured for diluted sample ($x = 0.01$). The above assumption is confirmed by the temperature dependence of measured lifetimes.

For all Dy^{3+} concentrations available the measured lifetimes increased with increasing temperature and this dependence is more pronounced in the case of higher doping levels. In Fig. 9 we present the examples of typical dependencies of measured lifetimes on temperatures in the 77–300 K range. These results indicate that the luminescence originating from the $^4F_{9/2}$ level of Dy^{3+} in this host is quenched

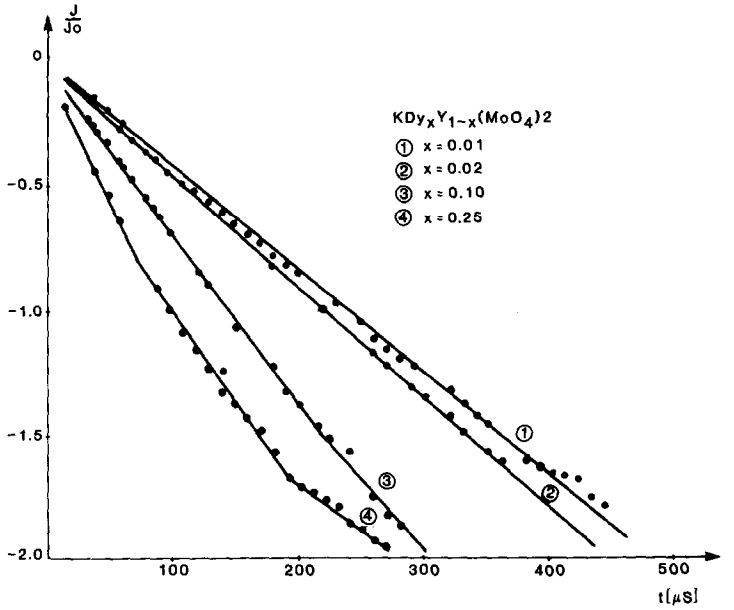

FIG. 8. Dy^{3+} ($^4F_{9/2} \rightarrow {}^4H_{13/2}$) emission decays as a function of the dysprosium concentration x (T = 300 K).

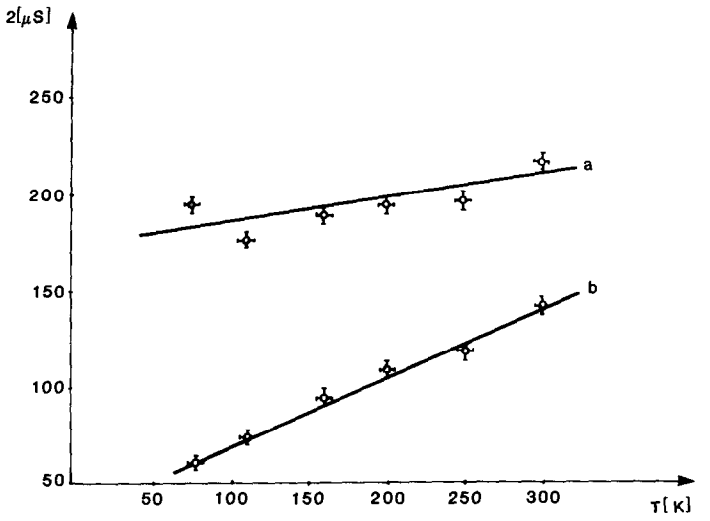

FIG. 9. Temperature dependence of Dy^{3+} lifetime for two dysprosium concentrations: (a) $x = 0.01$, (b) $x = 0.1$.

mainly by ion–ion interactions, which we assume to be the cross-relaxations via the $^4H_{5/2}$ level. The conditions for resonance are better fulfilled in the low-temperature limit. With increasing temperature the line broadening effects tend to destroy the resonance and to reduce the efficiency of the cross-relaxation process. The actual experimental data indicate that the electron–phonon coupling is weak in the crystal studied. However, the information we have is not sufficient for a detailed description of luminescence quenching in $KDy_xY_{1-x}(MoO_4)_2$ crystal. We believe that the time-resolved luminescence investigations, which are in preparation, will help to elucidate this problem.

From the slopes of the plots in Figs. 4 and 8 we derived the critical concentration. It amounts to 0.05 for Dy^{3+} and corresponds to the $R_0 = 9$ Å critical distance (*13*). This critical concentration can also be estimated from the intensity versus concentration plot. The concentration where the intensity starts to diminish and the decay times are reduced to 50% is $x = 0.05$. This value of x corresponds to a concentration of one ion per 4000 Å^3. This critical concentration compares reasonably well with the value obtained by van Uitert *et al.* (*14*) and Kellendonk and Blasse (*15*).

Magnetic Properties

Magnetic centers in the $KDy_xY_{1-x}(MoO_4)_2$ crystals, i.e., Dy^{3+} ions, decide the values of magnetic effects. Results of magnetic studies performed on fully concentrated $KDy(MoO_4)_2$ powdered samples are presented in Fig. 10 where the temperature functions of molar susceptibilities and their reciprocal values are illustrated. The obtained data fit best to the equation in the form $\chi_M = C/(T - \theta) + \chi_{TIP}$.

Reciprocal magnetic susceptibility of $KDy(MoO_4)_2$ is a linear function of temperature in the whole temperature range 4–293 K. A slight deviation of this function from linearity below 40 K results from crystal field effects. Therefore, the Curie–Weiss formula is obeyed for $\chi^{-1}(T)$ function in the range 40–293 K and the parameters determined from the linear part of the function are $\mu = 10.44$ BM and $\theta_p = 8.9$ K. All these facts indicate that exchange interactions in

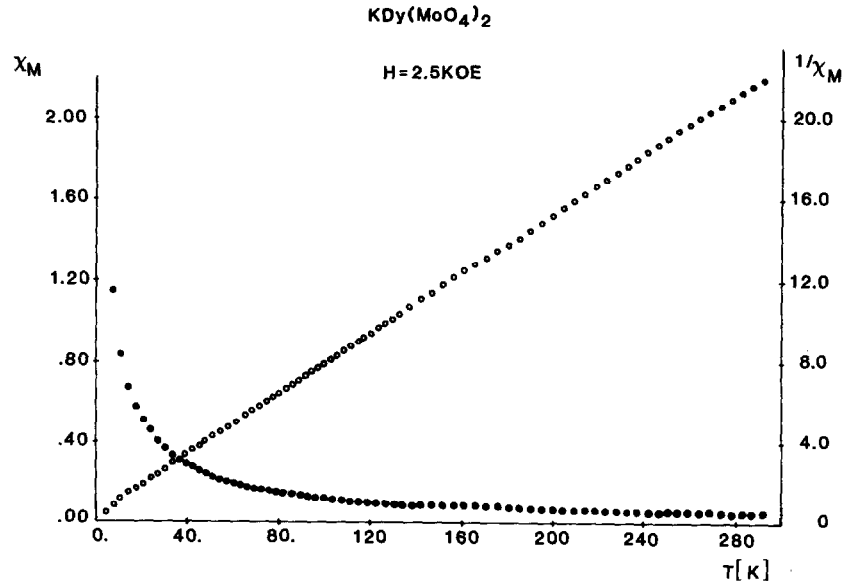

FIG. 10. The temperature dependence of molar susceptibility and inverse magnetic susceptibility for $KDy(MoO_4)_2$ polycrystalline sample.

$KDy(MoO_4)_2$ are weak and have no significant influence on the magnetic susceptibility. The room-temperature values of the magnetic susceptibilities are $\chi_g = 86.1 \times 10^{-6}$ and $\chi_M = 44.9 \times 10^{-3}$. They have no dependence on the magnetic field both in room and LHe temperatures. This fact indicates that the measured samples were free from any ferromagnetic contaminations and admixtures. The magnetic ordering was not detected in the whole temperature range which indicates that the orthorhombic phase of the $KDy(MoO_4)_2$ is stable down to LHe temperature and does not undergo any phase transition.

The magnetic data obtained for a single $KDy(MoO_4)_2$ crystal are presented in Table V. Magnetic parameters, e.g., Curie constant and g-factors, were calculated from the expression:

$$\chi = (Ng^2\beta^2/3kT)J(J + 1).$$

TABLE V

THE MAGNETIC ANISOTROPY OF $KDy(MoO_4)_2$ SINGLE CRYSTALS

Position of single crystal in magnetic field	Magnetic susceptibility		Magnetic[a] moment (BM)	Parameters calculated from magnetic data	
	gram $\chi \times 10^6$ ($cm^3\ g^{-1}$)	molar $\chi \times 10^6$ ($cm^3\ mole^{-1}$)		g factor	Curie constant
$a \parallel H$	85.6	44,700	10.2	1.28	13.1
$b \parallel H$	94.0	49,100	10.7	1.34	14.4
$c \parallel H$	109.0	56,900	11.5	1.45	16.7

[a] Magnetic moments were calculated from the expression $\mu_{eff} = 2.83\ (\chi_M T)^{1/2}$.

Examination of spectroscopic splitting parameters of $CaWO_4$ and $PbMoO_4$ with $RE_{0.5}Na_{0.5}$ admixtures (RE = Er, Tm, Yb, Tb, Dy, Ho) revealed their considerable anisotropy (*16*). The variations in the anisotropy from ion to ion are explained qualitatively by considering the effect of crystal field potential V_c on wave functions (J, M) for the free ions (*17, 18*). For Tb, Dy, and Ho, $g_\parallel > g_\perp$ was found, while for Er, Tm, and Yb, $g_\parallel < g_\perp$. It is so, because the ground states contain the high values of the axial quantum number M for Stevens constants α_J negative (Tb, Dy, Ho) and small numbers for α_J positive (Er, Tm, Yb) (*19–21*).

From the crystal structure of $KDy(MoO_4)_2$ it follows that its a, b, and c axes are nonequivalent crystallographically. The present studies revealed also the magnetic nonequivalence of crystals versus their axes. For that reason, in studies of the magnetic anisotropy of monocrystal, three crystallographic directions a, b, and c were considered, i.e., the crystal was placed in the magnetic field parallel to these axes. The main magnetic susceptibilities of $KDy(MoO_4)_2$ crystal have been measured. The effects, combined with anisotropy of the magnetic susceptibility, are as follows: $|K_1 - K_2| = 4400$, $|K_1 - K_3| = 12{,}200$, $|K_2 - K_3| = 7800$ (all values given in 10^{-6} cm^{-3} $mole^{-1}$ units).

Conclusions

The low-temperature magnetic and spectroscopic studies of $KDy_xY_{1-x}(MoO_4)_2$ crystals indicate that the orthorhombic phases of double lanthanide–potassium molybdates are stable up to LHe-temperature and do not undergo any phase transition. The unit cell structure is polymeric and built from MoO_6, LnO_8, and KO_{10} units. Dy^{3+} ions in $KDy_xY_{1-x}(MoO_4)_2$ have only one luminescent level, the quantum efficiency of which is close to unity for small Dy^{3+} concentrations. This level can be easily populated through strong pumping bands. However, it is depopulated by several radiative transitions whose luminescence branching ratios are nearly of the same order of magnitude. This is the main disadvantage of the crystal studies from the point of view of its application as a laser material.

References

1. L. F. JOHNSON AND H. J. GUGGENHEIM, *Appl. Phys. Lett.* **23,** 96 (1973).
2. A. A. KAMINSKI, P. V. KLEVTSOV, AND A. A. PAVLYUK, *Phys. Status Solidi A* **1,** K91 (1970); A. A. KAMINSKI, L. LI, A. A. PAVLYUK, P. V. KLEVTSOV, AND S. E. SARKISOV, *Neorg. Mater.* **9,** 2059 (1973); A. A. PAVLYUK, L. I. KOZEEVA, K. G. FOLIN, V. G. GLADYSHEV, V. S. GULYAEV, V. S. PIVTSOV, AND A. A. KAMINSKI, *Izv. Akad. Nauk SSSR Neorg. Mater.* **19,** 847 (1983).
3. R. F. KLEVTSOVA, L. P. KOZYEVA, P. V. KLEVTSOV, *Kristallography* **19,** 89 (1974); R. F. KLEVTSOVA, *Kristallography* **20,** 746 (1975); P. V. KLEVTSOV, W. A. WINOKUROV, AND R. F. KLEVTSOVA, *Kristallography* **18,** 1192 (1973); P. V. KLEVTSOV AND L. P. KOZYEVA, *Kristallography* **21,** 316 (1976); **20,** 1216 (1975).
4. J. HANUZA, AND V. V. FOMITSEV, *J. Mol. Struct.* **66,** 1 (1980); J. HANUZA AND L. ŁABUDA, *J. Raman Spectrosc.* **11,** 231 (1981); J. HANUZA AND L. MACALIK, *Spectrochim. Acta Part A* **38,** 61 (1982).
5. J. HANUZA, E. B. BURGINA, G. A. OSIPOVA, AND E. N. YURCHENKO, *J. Mol. Struct.* **158,** 141 (1987).
6. J. C. AXE AND G. H. DIEKE, *J. Chem. Phys.* **37,** 2364 (1962); H. M. CROSSWHITE AND G. H. DIEKE, *J. Chem. Phys.* **35,** 1535 (1961).
7. J. R. HENDERSON, N. MURAMOTO, AND T. M. HENDERSON, *J. Chem. Phys.* **47,** 5097 (1967).
8. W. T. CARNALL, P. R. FIELDS, AND K. RAJNAK, *J. Chem. Phys.* **49,** 4424 and 4412 (1968).
9. R. D. PEACOCK, *J. Chem. Soc. A,* 2028 (1971); *Mol. Phys.* **25,** 817 (1973).
10. N. A. KAZANSKAYA, *Opt. Spektrosk.* **29,** 1100 (1970).
11. C. V. BANKS AND D. W. KLINGMAN, *Anal. Chem. Acta* **15,** 356 (1956).
12. R. D. PEACOCK, *Struct. Bonding (Berlin)* **22,** 83 (1975).
13. R. K. WATTS, "Optical Properties of Ions in Solids," (B. Di Bartolo, Ed.), p. 307, Plenum, New York (1975).

14. L. G. VAN UITERT AND L. F. JOHNSON, *J. Chem. Phys.* **44,** 3514 (1966); L. G. VAN UITERT, E. F. DEARBORN, AND J. J. RUBIN, *J. Chem. Phys.* **45,** 1578 (1966); L. G. VAN UITERT, *J. Lumin.* **4,** 1 (1971).
15. F. KELLENDONK AND G. BLASSE, *Phys. Status Solidi B* **108,** 541 (1981).
16. L. HOLMES AND H. SCHIEBER, *J. Phys. Chem. Solids* **29,** 1663 (1968).
17. H. J. VAN VLECK, "The Theory of Electronic and Magnetic Susceptibilities," Oxford Univ. Press, London (1932).
18. W. G. PENNY, Schlapp.
19. R. J. ELLIOT AND K. W. H. STEVENS, *Proc. R. Soc. London, Ser. A* **219,** 387 (1953).
20. J. H. VAN VLECK, *Phys. Rev.* **41,** 208 (1932).
21. L. HOLMES AND M. SCHIEBER, *J. Appl. Phys.* **39,** 1200 (1968).